JOURNAL OF SOLID STATE CHEMISTRY 27, 87–97 (1979)

Alkali Metal Suboxides: Intermediates between Salts and Metals

A. SIMON

Max-Planck-Institut für Festkörperforschung, Heisenbergstrasse 1, 7000 Stuttgart 80, Germany

Received May 30, 1978

Rubidium and cesium form stable metal-rich oxides (suboxides) which have been investigated by thermal and structural analysis. The compounds Rb_9O_2, Rb_6O ($\triangleq Rb_9O_2Rb_3$), $Cs_{11}O_3$, Cs_4O ($\triangleq Cs_{11}O_3Cs_{10}$), $Cs_{11}O_3Rb$, and $Cs_{11}O_3Rb_7$ contain the characteristic ionic clusters Rb_9O_2 and $Cs_{11}O_3$. A simple model for the chemical bonding in alkali metal suboxides is described and proved by measuring the electrical properties and optical reflectivities as well as photoelectron spectra of these compounds. It is found that cesium suboxides play an important role in widely used photocathodes and image converters of type S1. The IR sensitivity of these devices is explained on the basis of surface plasmon-enhanced photoemission.

Introduction

Cesium suboxides have been known since 1909, when Rengade (*1, 2*) described the compounds Cs_7O, Cs_4O, Cs_7O_2, and Cs_3O. We undertook investigations of these substances, mainly for the purpose of understanding their very peculiar stoichiometries, which are not characteristic of alkali metals. The different aspects of our investigations are summarized briefly as follows.

(a) stable compounds: preparation, analysis, structure.

(b) Model of chemical bonding: electronic properties.

(c) The molten state, metastable phases.

(d) Application: IR photocathodes, thin films.

Discussion of (a) will be a recapitulation of well-known results for the sake of complete understanding. Recent results of physical measurements (b) shall then provide us with a quantitative understanding of chemical bonding as well as fascinating aspects of application of alkali metal suboxides (d).

Preparation and Structural Characterization of Stable Alkali Metal Suboxides

The alkali metal suboxides are prepared by reacting known amounts of oxygen, made by thermal decomposition of HgO with alkali metal in a glass apparatus (*3*). This apparatus is suitable equipped with gauges to control the vigorous reaction. Specially designed, very tiny glass devices, which can be attached to the main apparatus, allow safe handling of the samples, e.g., when taking samples for X-ray investigations, etc.

Thermal analysis data lead to a revised phase diagram of the cesium–oxygen system (*3*). The results, summarized in Table I, are in accordance with Rengade's early results,

TABLE I

BINARY ALKALI METAL SUBOXIDES (*3*)

This work	Cs_7O	Cs_4O	$Cs_{11}O_3$	$Cs_{3.1-3.6}O$
Rengade (*1, 2*)	Cs_7O	Cs_4O	(Cs_7O_2)	(Cs_3O)
This work	Rb_6O	Rb_9O_2		
Touzain (*4, 5*)		(Rb_3O)		

0022-4596/79/010087-11$02.00/0

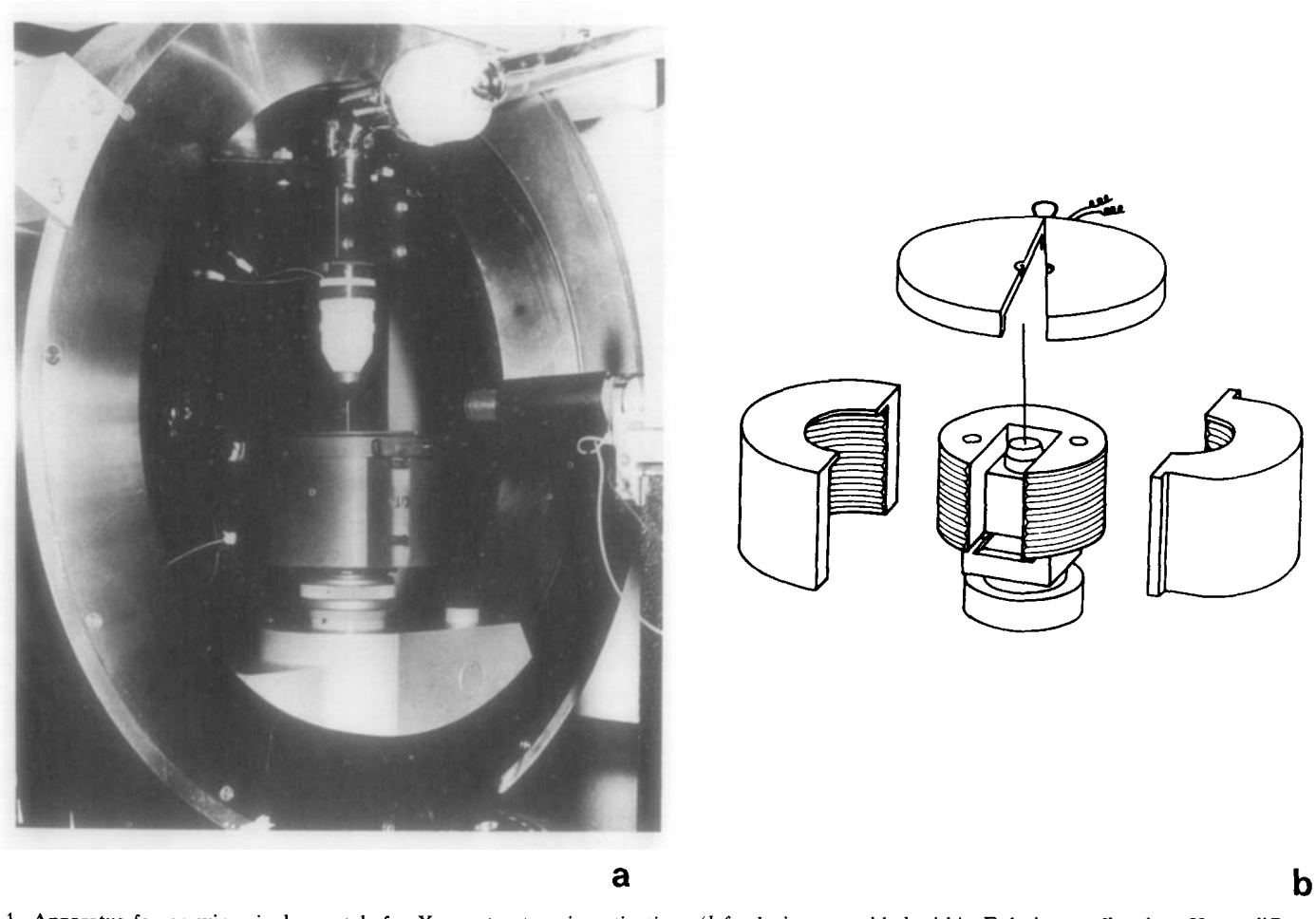

FIG. 1. Apparatus for growing single crystals for X-ray structure investigations (*left*: device assembled within Eulerian cradle of an X-ray diffractometer; *right*: disassembled after crystal growth.)

except for the oxygen-rich compounds. The metal rubidium also forms suboxides. Because of the very close proximity of thermal effects the phase relationships in the Rb/O system are rather difficult to determine. One of the compounds (Rb_9O_2) was found independently by Touzain (*4, 5*) but was analyzed as Rb_3O.

The different formula had to be verified, analyzed, and understood by means of X-ray investigations. For this purpose, special equipment was developed: (a) a continuously working camera for low-temperature work on the basis of the Guinier-technique (*6*), and (b) an even more essential small device for growing single crystals of low-melting or decomposing substances *in situ* directly on the diffractometer spindle (Fig. 1). The capillary, filled with liquid sample, reaches into the cold nitrogen stream through a heatable metal screen. Rotation of the inner part moves the screen down slowly, thus introducing more and more of the capillary into the cold gas stream. This leads to the growth of single crystals, which can be investigated after disassembling the whole device.

Investigation of these crystals at low temperatures led to a very consistent structure principle (*8*): The O atoms are always surrounded octahedrally by metal atoms; two such octahedra may be linked via common faces, which leads to the Rb_9O_2 cluster, or three face-sharing octahedra may form the $Cs_{11}O_3$ cluster. This is demonstrated for the compound Rb_9O_2 (Fig. 2a), which consists only of close-packed Rb_9O_2 clusters (*9*), and for the compound $Cs_{11}O_3$ (Fig. 3a), which is again composed of $Cs_{11}O_3$ clusters (*10*) in a close-packed arrangement. The atomic distances within the clusters are the same as those in the normal oxides M_2O, whereas the distances between the clusters are nearly the same as those in the pure metals. These facts are discussed on the basis of a very simple bonding model, assuming normal valencies of the metals and oxygen. One arrives at the positively charged clusters $(Rb_9O_2)^{5+}$ and $(Cs_{11}O_3)^{5+}$. In the electrically neutral compounds five electrons provide the metallic bonding between the clusters. In such a sense we are dealing with "complex metals," with the simple ion of a normal metal substituted by the complex ion groups.

Such clusters may combine with additional alkali metal to form compounds of new stoichiometries. This principle is illustrated for the compound Rb_6O in Fig. 2b. Here, Rb_9O_2 clusters are arranged in layers, alternating with intermediate layers of pure rubidium

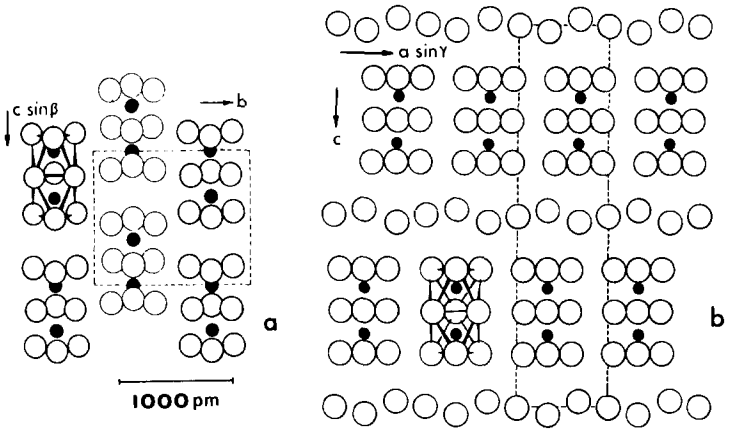

FIG. 2. Crystal structures of (a) Rb_9O_2 (monoclinic, projected along [001]) and (b) Rb_6O (hexagonal, projected along [100]). The unit cells are outlined; metal atoms are drawn as open circles.

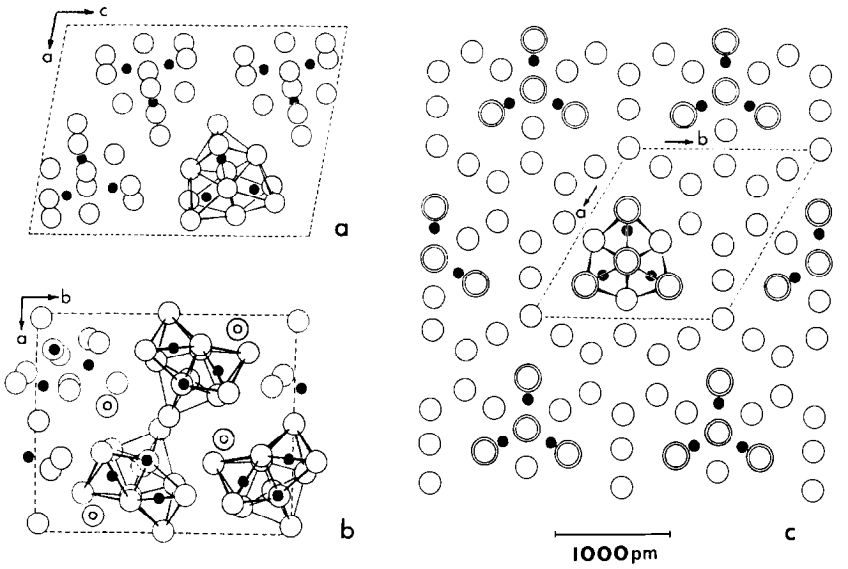

FIG. 3. Crystal structures of (a) $Cs_{11}O_3$ (monoclinic, projected along [010]), (b) Cs_4O (orthorhombic, projected along [001], single Cs atoms indicated by an inner circle) and (c) Cs_7O (hexagonal, projected along [001]). The unit cells are outlined; metal atoms are drawn as open circles.

(*11*). In Cs_7O (Fig. 3c) the $Cs_{11}O_3$ cluster is incorporated in a matrix of pure cesium (*12*). This matrix of additional cesium atoms is minimized to just one additional "metallic" cesium atom in the case of Cs_4O (Fig. 3b) (*7*). The intermediate cesium atoms are substituted by Rb atoms in the compound $Cs_{11}O_3Rb$, leading to a rearrangement of the clusters (*13*). It is obvious that, in this compound, the chemically very similar elements Rb and Cs behave quite differently. The compound $Cs_{11}O_3Rb_7$ provides another such example, where—by simply oxidizing an alloy of Rb and Cs—one can completely separate the metals in space (*14*). The last two examples beautifully illustrate the intermediate position of alkali metal suboxides between salt-like and metallic-type bonding, separated in space in a very unique way.

Molten State and Metastable Phases

All suboxides described so far are characterized by the occurrence of typical ion clusters. Do these clusters also occur in the melt? Investigations of this question have just been started, and a definite answer cannot be given yet, but the information on the melt gained so far is very interesting and promises a detailed answer. Because of experimental difficulties, it took some time to measure the Raman spectra of these metallically reflecting suboxides (*15, 16*). These spectra are shown in Fig. 4, including the spectrum of a liquid Cs_7O sample. All spectra exhibit great similarities despite the fact that the crystal structures of the investigated compounds are rather different. The occurrence of the $Cs_{11}O_3$ cluster in all compounds suggests that one may ascribe the bands to the characteristic modes of this cluster. Assignment of the bands to definite vibrational modes have not yet been made, but the spectrum of liquid Cs_7O (as well as the spectrum of liquid $Cs_{11}O_3Rb_7$) looks very similar to the spectrum of the solid cesium suboxides. So one might draw the conclusion that the same ion clusters as those in the solid are occurring in the melt.

Neutron diffraction investigations of the molten suboxides provide results which are

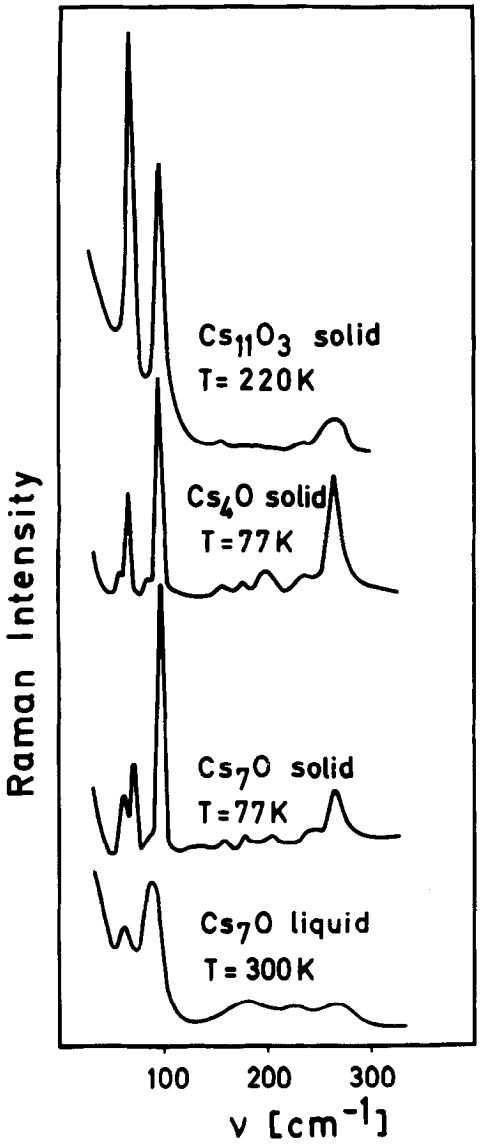

FIG. 4. Raman spectra of solid and liquid cesium suboxides.

clearly correlated to the structure of the solids (*17*): The scattering function of liquid Rb is drastically altered by the addition of oxygen. The radial distribution function of the liquid suboxide Rb_6O reveals pair distributions which are very similar to the interatomic distances in solid Rb_6O.

Somewhat contradictory with respect to the occurrence of the typical ion clusters are the results of an investigation of a metastable (quenched) phase in the rubidium oxygen system (*18*). Rapid quenching of a melt of composition Rb_7O to the temperature of liquid nitrogen leads to solidification into an amorphous phase. Upon heating, a new intermediate crystalline phase occurs. Because formation and decomposition of that phase are exothermic processes, this intermediate phase must be metastable. At 180°K it decomposes into a mixture of Rb and Rb_9O_2; the reaction path is shown in Fig. 5. The metastable phase has the most probable composition $Rb_{6.33}O$, where the Rb atoms in the structure are arranged in centered icosahedra. But this is only one way of looking at the structure, which is shown in Fig. 6a. Seeking the possible positions of oxygen atoms, which could not be located directly, one visualizes a framework of isolated Rb_6 octahedra which are metallically bound to one another and to intermediate Rb atoms in very much the same manner as that with the stable suboxides. Thus the formula $Rb_{6.33}O$ corresponds to a structure $(Rb_6O)_3Rb$. From this result one might draw the conclusion that Rb_9O_2 clusters are not the dominant species in the melt of composition Rb_7O, although one has to be careful with such a conclusion, as nucleation could be a very selective process changing the species in the quenched phase.

Chemical Bonding and Electronic Properties of Alkali Metal Suboxides

Assuming normal valencies (1+ for Rb and Cs, 2− for O), one arrives at a picture of chemical bonding in alkali metal suboxides characterized by the occurrence of charged ion clusters linked to one another by metallic bonding. This model has to be proved, first in a qualitative way by ensuring the metallic properties of all alkali metal suboxides, and then in a quantitative way by determination of the number of free carriers in these compounds.

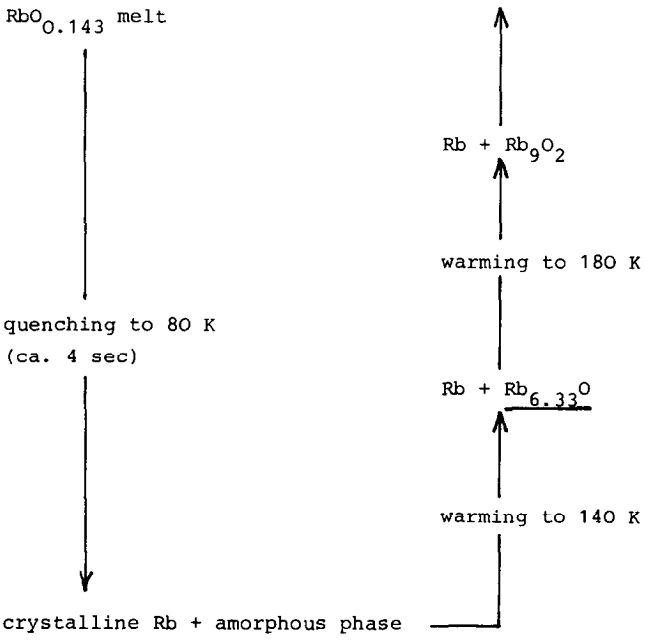

FIG. 5. Relations of the metastable phase $Rb_{6.33}O$ to other phases in the Rb/Rb_2O system (*18*).

The temperature dependence of the specific resistivity for a number of samples (*19*) measured with a contactless method (*20*), is shown in Fig. 7. The values are in rather good agreement with some earlier measurements by Brauer (*21*). All compounds are metals. Except for the mixed compound $Cs_{11}O_5Rb_7$ one finds convincingly high values of the residual resistivity ratio, which, after subtraction, leads to a temperature dependence of resistivity very similar to that found in the pure metals Rb and Cs: At

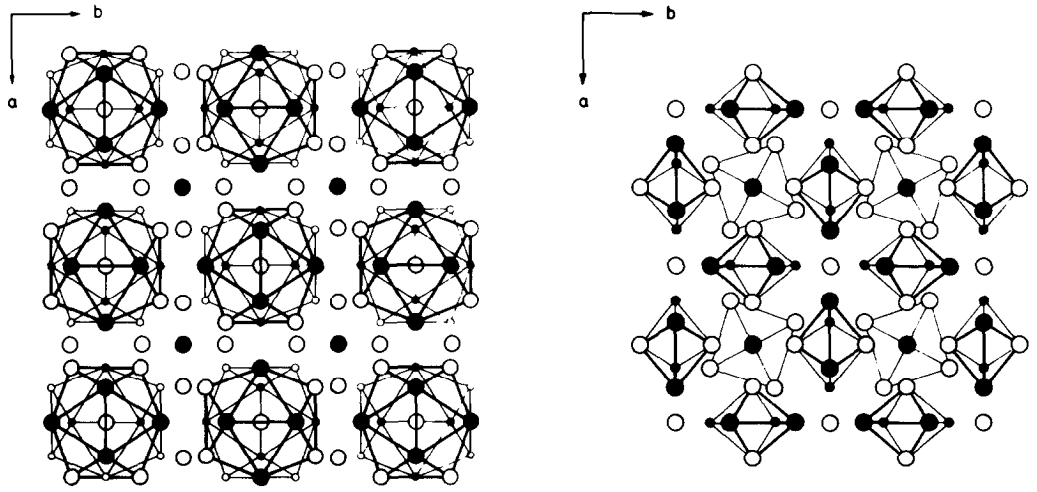

FIG. 6. Crystal structure of $Rb_{6.33}O$ (unit cell content $Rb_{152}O_{24}$). (a) All nearest-neighbour Rb–Rb distances are drawn (centered icosahedra of Rb atoms) (b) The same structure is drawn as an arrangement of isolated Rb_6 octahedra (around oxygen atoms).

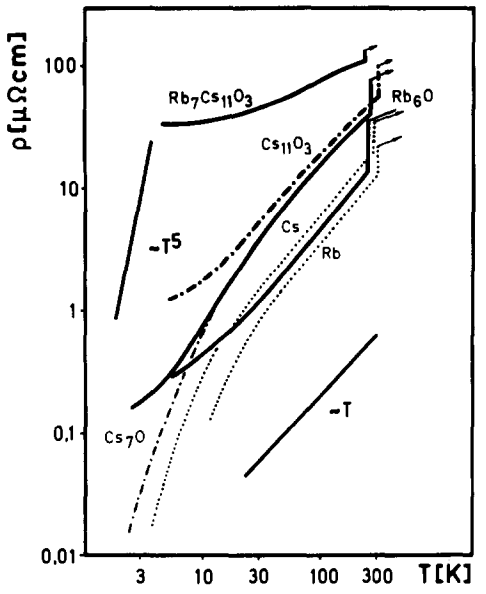

FIG. 7. Electrical resistivity of Rb, Cs, Cs_7O, $Cs_{11}O_3$, $Cs_{11}O_3Rb_7$, and Rb_6O as function of temperature.

high temperature ρ is proportional to T; at low temperature it approaches the T^5 law. The suboxides therefore behave as free electron-like metals.

A first quantitative proof of the bonding model is gained by looking at a very obvious property of the compounds, their beautiful colours. Rb_9O_2 looks like copper, and Cs_7O is bronze-coloured; further oxidation leads to violet Cs_4O and violet-blue $Cs_{11}O_3$, until a greenish-black color is reached with the homogeneous phase "Cs_3O."

There is a simple straightforward explanation for these color changes (*22*). According to reflectivity measurements (Fig. 8), the plasma edge is shifted to lower energy with rising oxygen content. This behavior is expected, as electrons are trapped at the oxygen atoms, and so the free electron concentration decreases upon oxidation. The evaluation of free electron concentrations from the measured plasma frequencies according to $\omega = [4\pi(e^2/m) \cdot N]^{1/2}$ (e = unit charge, m = effective mass) leads to a fair agreement between calculated and expected values of N: The free electron concentration

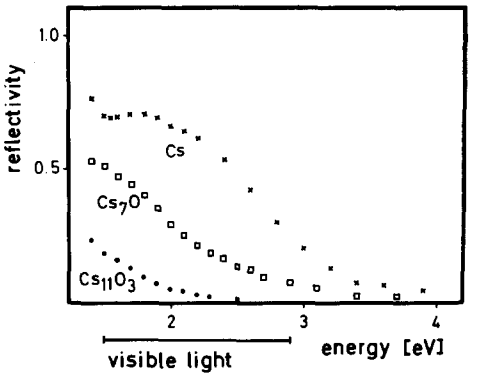

FIG. 8. Reflectivity of metallic samples Cs, Cs_7O, and $Cs_{11}O_3$.

per formula unit (n) is 13.5 in the case of $Cs_{11}O_3Cs_{10}$ and 3.5 in the case of $Cs_{11}O_3$ (instead of 15 and 5, respectively). The derived values of n are still rather inaccurate, mainly because of the restricted range of the spectrum available in the measurements. Therefore, no correction terms have been applied to the reflectivity data. A more complete treatment will be given in connection with UPS measurements.

Photoelectron spectroscopy with alkali metal suboxides was first started using an X-ray source (ESCA). But it soon became evident that, because of resolution problems, it was necessary to use UV sources (UPS). As UPS is a very surface-sensitive method, providing information about surface layers of 10- to 20-Å thickness, it was necessary to prepare and investigate the extremely air-sensitive samples under UHV conditions (basis pressure below 10^{-10} Torr). Measurements were done using He I, II and Ne I, II resonant sources (*23*). Some He I spectra are plotted in Fig. 9. For these investigations, only congruently melting samples Rb, Cs, Cs_7O, and $Cs_{11}O_3Rb$ were chosen.

Clearly the metallic nature of all samples is expressed by the partly filled conduction band. Upon oxidation, a very sharp peak arises at low binding energy, which must be attributed to the emission from the O 2*p*

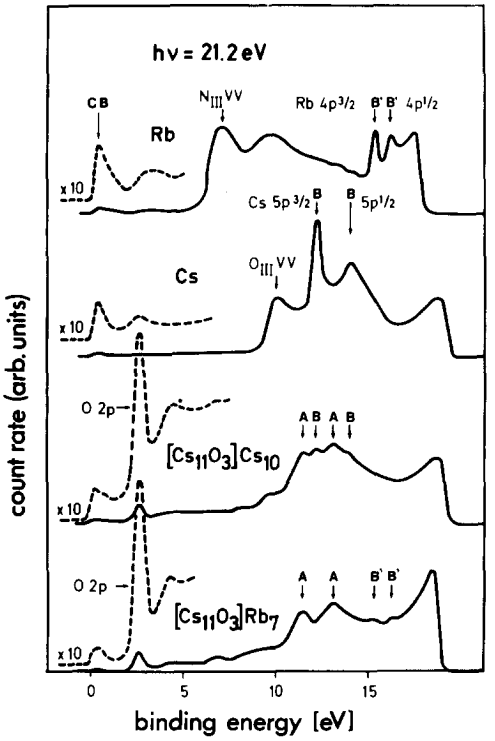

FIG. 9. HE I photoelectron spectra of Rb, Cs, $Cs_{11}O_3Cs_{10}$ ($\triangleq Cs_7O$), and $Cs_{11}O_3Rb_7$. The inscriptions are explained in the text.

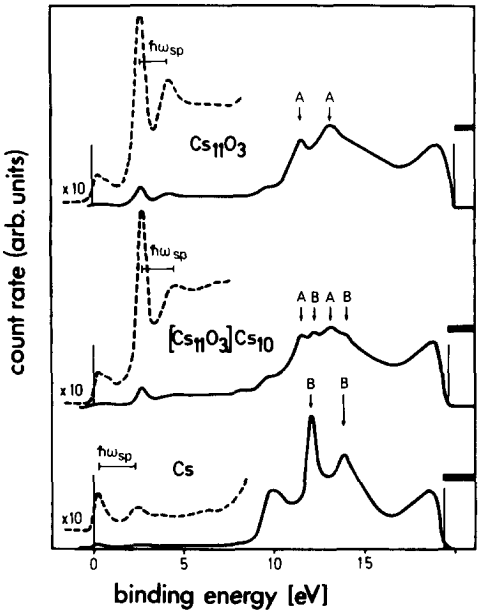

FIG. 10. He I photoelectron spectra of $Cs_{11}O_3$, $Cs_{11}O_3$ Cs_{10}, and Cs. The inscriptions are explained in the text.

level. Both the extremely narrow structure of 0.6 eV (normally occurring with fully occupied cored levels) and the extraordinarily low binding energy of 2.7 eV clearly indicate the occurrence of O^{2-} ions in suboxides. The electronic levels of the metal atoms also change drastically. The spin–orbit–split Cs $5p$ level of cesium develops into a quadruple structure in the case of $Cs_{11}O_3Cs_{10}$: Part of the emission occurs at the same energies as with the metal, and part is shifted to lower binding energies. The shifted Cs $5p$ doublet occurs as a result of photoemission from the cluster atoms. This assignment is verified by the spectrum of $Cs_{11}O_3Rb$, which only contains cesium in the ion clusters and, therefore, only contains the shifted Cs $5p$ doublet. A further verification of the assignment is given by a chemical reaction in the spectrometer. As shown in Fig. 10, thermal decomposition of $Cs_{11}O_3Cs_{10}$ leads to the crystallization of $Cs_{11}O_3$ (at room temperature) in accordance with phase studies of bulk materials. Again only the shifted Cs $5p$ doublet occurs with $Cs_{11}O_3$.

Finally, the spectra yield a further very interesting conclusion. It is well known that electrons passing through a metal are capable of exciting plasma oscillations. So the photo electrons—on their way to the surface—create plasma oscillations, while losing the equivalent amount of kinetic energy. Therefore, all peaks in the UPS spectra are accompanied by energy loss peaks at lower kinetic energy (corresponding to a higher binding energy). When taking the lowest excitation energy of He I with the associated very small electron escape depth, it became evident that the energy loss peaks were due to the formation of surface plasmons. The energy difference between a main peak and the correlated energy loss peak is identical to the surface plasmon energy. On the basis of a formalism very similar to that

TABLE II

CONCENTRATION OF FREE ELECTRONS IN ALKALI METAL SUBOXIDES FROM UPS ACCORDING TO $\hbar\omega_{sp} = \{e^2/[(2+\Delta\varepsilon_c)\pi \cdot m]\}N$

			u (per formula unit)	
	$\hbar\omega_{sp}$	$N(\times 10^{21})$	Observed	Expected
Cs	2.0	6.9	1.0	1
$Cs_{11}O_3Cs_{10}$	1.75	5.4	14.9	15
$Cs_{11}O_3$	1.55	4.3	5.5	5

Definitions of variables: $\hbar\omega_{sp}$, surface plasmon energy; e, unit charge; $\Delta\varepsilon_c$, core polarizability; m, effective electron mass; N, free electron concentration per cm^{-3}.

already used in conjunction with the metallic reflectivity, the free electron concentration can be evaluated from the measured value of the surface plasmon energy. A more complete treatment must be taken into account, e.g., deviations of effective mass from unity as well as core polarizabilities. The measured values of the surface plasmon energy and the free carrier concentrations n_0 are listed in Table II. The electron concentration with the suboxides $Cs_{11}O_3Cs_{10}$ and $Cs_{11}O_3$ relative to n_0 (Cs) = 1 are in very good agreement with the expected values, leading to a quantitative proof of the simple picture of chemical bonding.

Application: The Infrared-Sensitive S1 Photocathode

It has been known for about 50 years (*24*) that composite layers of Cs_2O and Cs play an important role in photocathodes, which are sensitive in the IR region. The application of such devices ranges from intensity measurements in the near IR to image converters, which change an invisible IR picture to a visible one. Such a device, based on thin films of Cs and Cs_2O on a silver substrate, is drawn schematically in Fig. 11. Many explanations for the infrared photoemission process of such a cathode have been put

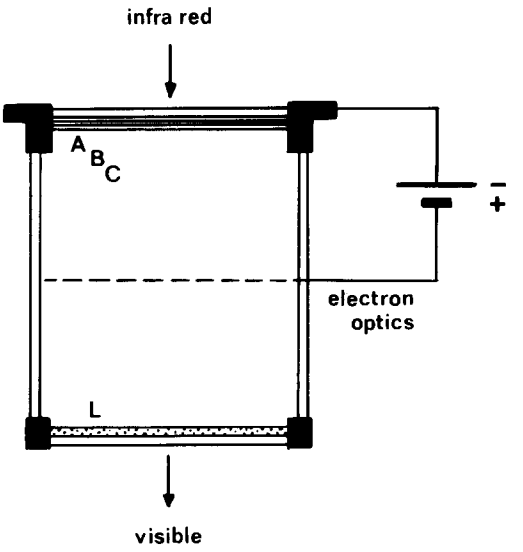

FIG. 11. Schematic view of an IR image converter on the basis of an S1 photo cathode. (*ABC*: composite layer of Ag, Cs_2O, and Cs; $B + C$ is assumed to react to form suboxides.)

forward on the basis of separate layers, but as a result of our work on the bulk system we could not believe in the existence of separate Cs and Cs_2O layers. One would expect a reaction leading to a suboxide layer. Indeed, the photoelectric yield curves of such cathodes can be explained on the basis of the photoemission properties of cesium suboxides.

If we consider the behavior of a normal metal, e.g., Al, we find that its photoelectric yield curve is characterized by the onset of photoemission at ~4.2 eV (work function of Al). The yield then develops into a maximum at ca. 10.5 eV (energy of surface plasmon). Thus the decay of surface plasmons enhances the photoelectric yield.

Because the metal cesium is characterized by values of both the work function (1.94 eV) and the surface plasmon energy (2.00 eV) much lower than those of aluminum, photoelectrons are emitted at much lower energies. These values decrease further upon oxidation of cesium. This has already been shown for the surface plasmon energy which

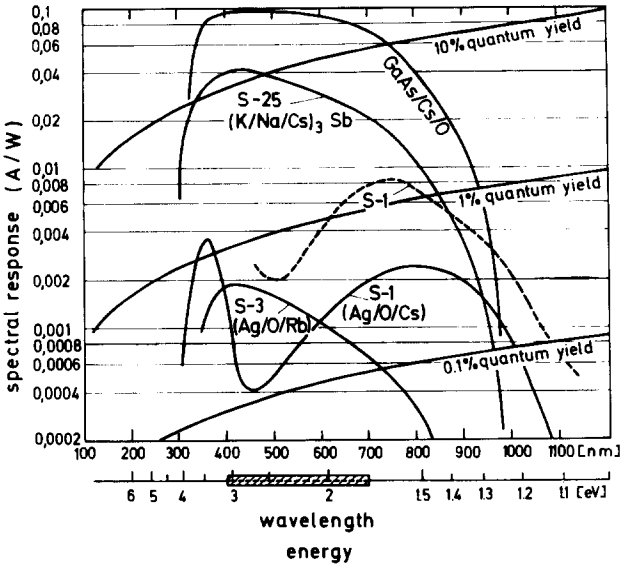

FIG. 12. Photoelectronic yield curves of some commercial photo cathodes.

decreases to a value $\omega_{sp} = 1.55$ eV, but it also holds for the work function. The values for the work functions can be extracted from Fig. 12: Only electrons with a kinetic energy larger than or equal to the work function of the sample are ejected into the vacuum, which causes the gap between excitation energy (21.2 eV) and the beginning of the photoemission in the photoelectron spectra. As easily seen in Fig. 10, this gap becomes smaller with increasing oxygen content of the sample. In the case of $Cs_{11}O_3$ the work function reaches a value of less than 1.4 eV. If these data are compared with the yield curves of S1 photocathodes, the photoemission data of $Cs_{11}O_3$ explain perfectly the maximum near 1.6 eV, responsible for the photoemission in the near-infrared region as due to surface plasmon decay (*25*).

Of course, there is a strong argument against such an explanation: These surface layers have a thickness of a few atomic diameters. One might question the existence of a chemical compound like $Cs_{11}O_3$ in such a layer, as well as the assertion that the electronic properties of such a thin layer are comparable to the properties derived from the bulk sample. But we were able to show that a thin film of roughly two to three monolayers of cesium atoms, when oxidized, develops a photoelectron spectrum which is identical to that of a bulk suboxide sample (*25*).

Acknowledgments

The very efficient and pleasant cooperation of H.-J. Deiseroth, W. Brämer, E. Westerbeck (preparation and structures), W. Bauhofer (electrical resistivity), C. Mack (reflectivity), and G. Ebbinghaus and W. Braun (UPS) is gratefully acknowledged. The work was supported by Deutsche Forschungsgemeinschaft and Fonds der Chemischen Industrie.

References

1. E. RENGADE, *Bull. Soc. Chim. France [4]* **5**, 994 (1909).
2. E. RENGADE, *C.R. Acad. Sci. Paris* **148**, 1199 (1909).
3. A. SIMON, *Z. Anorg. Allg. Chem.* **395**, 301 (1973).
4. PH. TOUZIAN, *Canad. J. Chem.* **47**, 2639 (1969).
5. PH. TOUZAIN AND M. CAILLET, *Rev. Chim. Minér.* **8**, 277 (1971).
6. A. SIMON, *J. Appl. Crystallogr.* **4**, 138 (1971).

7. A. SIMON, H.-J. DEISEROTH, E. WESTERBECK, AND B. HILLENKÖTTER, *Z. Anorg. Allg. Chem.* **423**, 203 (1976).
8. A. SIMON, *in* "Crystal Structure and Chemical Bonding in Inorganic Chemistry" (C. J. M. Rooymans and A. Rabenau, Eds.), p. 47, North–Holland, Amsterdam (1975).
9. A. SIMON *Z. Anorg. Allg. Chem.* **431**, 5 (1977).
10. A. SIMON AND E. WESTERBECK, *Z. Anorg. Allg. Chem.* **428**, 187 (1977).
11. A. SIMON AND H.-J. DEISEROTH, *Rev. Chim Minér.* **13**, 98 (1976).
12. A. SIMON, *Z. Anorg. Allg. Chem.* **422**, 208 (1976).
13. H.-J. DEISEROTH AND A. SIMON, to be published.
14. A. SIMON, W. BRÄMER, AND H.-J. DEISEROTH, *Inorg. Chem.*, in press.
15. G. EBBINGHAUS, Thesis, Stuttgart (1977).
16. H. J. STOLTZ AND G. EBBINGHAUS, *Verhandl. Deut. Pathol. Ges. (VI)* **12**, 309 (1977).
17. J. R. D. COPLEY AND A. SIMON, to be published.
18. H.-J. DEISEROTH AND A. SIMON, *Z. Naturforsch.*, in press.
19. W. BAUHOFER AND A. SIMON, *Z. Anorg. Allg. Chem.*, in press.
20. W. BAUHOFER, *J. Phys.* **10**, 1212 (1977).
21. G. BRAUER, *Z. Anorg. Chem.* **255**, 101 (1947).
22. K. MACK AND A. SIMON, to be published.
23. G. EBBINGHAUS, W. BRAUN, AND A. SIMON, *Z. Naturforsch. B* **31**, 1219 (1976).
24. L. R. KOLLER, *J. Opt. Soc. Amer.* **19**, 135 (1929).
25. G. EBBINGHAUS, W. BRAUN, A. SIMON, AND K. BERRESHEIM, *Phys. Rev. Lett.* **37**, 1770 (1976).